Results in Physics 8 (2018) 545–551

Contents lists available at ScienceDirect

Results in Physics

journal homepage: www.journals.elsevier.com/results-in-physics

Exploring magnetic dipole contribution on radiative flow of ferromagnetic Williamson fluid

T. Hayat [a,b], Salman Ahmad [a,*], M. Ijaz Khan [a], A. Alsaedi [b]

[a] Department of Mathematics, Quaid-I-Azam University, 45320 Islamabad 44000, Pakistan
[b] Nonlinear Analysis and Applied Mathematics (NAAM) Research Group, Department of Mathematics, Faculty of Science, King Abdulaziz University, P.O. Box 80257, Jeddah 21589, Saudi Arabia

ARTICLE INFO

Article history:
Received 2 November 2017
Received in revised form 23 November 2017
Accepted 25 November 2017
Available online 27 December 2017

Keywords:
Ferromagnetic Williamson liquid
Magnetic dipole
Thermal radiation
Viscous dissipation

ABSTRACT

The purpose of present article is to analyze the impacts of thermal radiation and magnetic dipole in flow of ferromagnetic Williamson liquid over a stretched surface. Appropriate transformations are utilized to obtain the relevant nonlinear differential system. The obtained differential system is tackled numerically with the help of built-in-shooting method. Influence of viscous dissipation, ferromagnetic interaction parameter, cure temperature, Prandtl number, Weissenberg number (material parameter) and thermal radiation are observed on temperature and velocity fields. Further velocity and temperature gradients are discussed and analyzed graphically. The obtained outcomes declare that surface drag force and heat transfer rate enhance for higher estimation of thermal radiation and Prandtl number. Moreover velocity field decays verses Weissenberg number.

© 2017 Published by Elsevier B.V. This is an open access article under the CC BY-NC-ND license (http://creativecommons.org/licenses/by-nc-nd/4.0/).

Introduction

Ferrofluids (portmanteau of liquid and ferromagnetic particles) is a liquid in the presence of external magnetic field that becomes magnetized. These types of fluids are liquids colloidal made by nanoscale ferrimagnetic or ferromagnetic particles suspended in a fluid carrier (usually an water or organic solvent). The suspension of particles is caused by Brownian motion and under normal condition these particles will not settle. Further every ferromagnetic particles are coated by surfactant to prevent the clumping. Magnetic attraction of nanoscale ferromagnetic particles is low when surfactant van der Waals force of sufficient strength to inhibit agglomeration or magnetic clumping. There are various application of ferromagnetic fluids. For example in electronic devices, analytical instrumentation, medicine, friction-reducing agent, angular momentum change agent, heat transfer agent etc. Due to these uncountable applications many scientists and researchers accelerated the study of ferrofluid. Firstly Anderson and Vanes [1] studied effect of magnetic dipole on ferrofluid. Titus and abraham [2] investigated ferroliquid flow and heat transfer past a stretchable sheet. Effect of thermal radiation on ferrofluid in the presence of magnetic dipole is explored by Zeeshan et al. [3]. Interaction of ferromagnetic fluid flow with convective heat transfer is discussed by Sheikholeslami et al. [4]. Neuringer [5] discussed magnetic dipole impact on stagnation point flow against a heated ferrofluid flow towards a wall with linearly decreasing surface temperature. Kefati [6] accomplished convective flow of ferromagnetic liquid with linear temperature in a cavity. He verified that by adding the ferromagnetic particles heat transfer rate decays. They concluded that Nusselt number directly depends upon Reynolds number and volume fraction, while Hartmann number has opposite behavior. Few recent articles related to ferrofluid flow are presented by Refs. [7–15].

Radiation effect has several applications in engineering, physics and industry like glass production, polymer processing, space technology and in nuclear reactors. Sunlight also known as solar radiation is a form of radiation that obtained from the sun. Sun/solar energy never runs out, no burning or motion are required in the energy conservation process. Few recent investigations on radiative flow can be found in Refs. [16–24].

Many biological liquids together with the liquids are utilized in industrial utilizations like printer ink, detergents, animal bloods, paints, polymer liquids, food stuff etc. The Naver-Stokes equation is incapable to elucidate the rheological feature of non-Newtonian fluid. In order to elucidate such types of features several fluid models have been suggested. Few suggested models are Ellis model, Carreau model, Cross model, power law model etc. In such types of models there is one known as the Williamson model. Williamson [25] experimentally proposed a model for the

* Corresponding author.
E-mail address: salmanuom206@gmail.com (S. Ahmad).

https://doi.org/10.1016/j.rinp.2017.11.040
2211-3797/© 2017 Published by Elsevier B.V.
This is an open access article under the CC BY-NC-ND license (http://creativecommons.org/licenses/by-nc-nd/4.0/).

description of pseudoplastic fluid flow. Hayat et al. [26] investigated flow of Williamson fluid with Soret-Dufour effects and thermal radiation. Yousaf et al. [27] explored three dimensional flow of Williamson fluid. Zahra et al. [28] presented numerical simulation for flow of Williamson fluid with variable viscosity. Further some investigations covering Williamson liquid we addressed through the Refs. [29–34].

Present work is aimed to investigate Williamson ferrofluid flow over a stretchable sheet under the impacts of magnetic dipole and thermal radiation. Viscous dissipation is also accounted. By a suitable similarity transformation procedure the governing partial differential equations are transformed into ordinary differential equations. The resulting ODE's are solved numerically by standard Shooting method [35–40]. The obtained consequences are comprehensively discussed.

Description of problem

Here two-dimensional (2D) ferromagnetic flow of Williamson liquid is modeled. Heat transfer modeling is performed by considering thermal radiation and viscous dissipation. For magnetization of liquid magnetic dipole of sufficient strength is placed at a distance a below x-axis and center on y-axis (see Fig. 1). Temperature of sheet denoted by T_w which is less then T_c where T_c is ambient temperature. The governing flow expressions are

$$\nabla \cdot \mathbf{V} = 0, \tag{1}$$

$$\rho \frac{d\mathbf{V}}{dt} = -\nabla p + \nabla \tau + \lambda_0 (\mathbf{M} \cdot \nabla)\mathbf{H}, \tag{2}$$

$$\rho c_p \frac{dT}{dt} + \lambda_0 T \frac{\partial M}{\partial T}(\mathbf{V} \cdot \nabla) H = k\nabla^2 T - \nabla \cdot \mathbf{q} + \tau : \mathbf{L}, \tag{3}$$

here $\mathbf{q}$ indicates radiative heat flux and $\mathbf{L}$ the velocity gradient.

Cauchy stress tensor for Williamson liquid model is [32]:

$$\tau = \left[\mu_\infty + \frac{\mu_0 - \mu_\infty}{1 - \Gamma|\dot{\gamma}|}\right]\mathbf{A}_1, \tag{4}$$

where

$$\mathbf{A}_1 = \mathbf{L} + \mathbf{L}^T, |\dot{\gamma}| = \sqrt{\frac{1}{2} trace(A_1^2)} = \sqrt{\left[2\left(\frac{\partial u}{\partial x}\right)^2 + 2\left(\frac{\partial v}{\partial y}\right)^2 + \left(\frac{\partial u}{\partial y} + \frac{\partial v}{\partial x}\right)\right]}, \tag{5}$$

in which μ_0 and μ_∞ denote the low and high shear rates viscosities, Γ the material time constant, A_1 the first order Rivlin-Erickson tensor and $\dot{\gamma}$ the shear rate. Present flow can be put into the following expressions [8,10]:

$$\frac{\partial u}{\partial x} + \frac{\partial v}{\partial y} = 0, \tag{6}$$

$$\begin{aligned} &u\frac{\partial u}{\partial x} + v\frac{\partial u}{\partial y} = v\frac{\partial^2 u}{\partial y^2} + 2v\Gamma\frac{\partial u}{\partial y}\frac{\partial^2 u}{\partial y^2} + \frac{\lambda_0 M}{\rho}\frac{\partial H}{\partial x}, \\ &\rho c_p\left(u\frac{\partial T}{\partial x} + v\frac{\partial T}{\partial y}\right) + \lambda_0 T\frac{\partial M}{\partial T}\left(u\frac{\partial H}{\partial x} + v\frac{\partial H}{\partial y}\right) \\ &\quad = k\frac{\partial^2 T}{\partial y^2} - \frac{\partial q_r}{\partial y} + \mu_0\left[\left(\frac{\partial u}{\partial y}\right)^2 + \Gamma\left(\frac{\partial u}{\partial y}\right)^3\right], \end{aligned} \tag{7}$$

with

$$u|_{y=0} = cx, v|_{y=0} = 0, T|_{y=0} = T_w, u|_{y\to\infty} \to 0, T|_{y\to\infty} \to T_c. \tag{8}$$

here u and v represent the velocity components, v the kinematic viscosity, Γ the material time variables, λ_0 the magnetic permeability, ρ the density, M the magnetization, H the magnetic field, c_p the specific heat, T the fluid temperature, k the thermal conductivity, μ_0 the limiting viscosities at zero shear rate and q_r the component of radiative flux $\mathbf{q}$.

Employing Rosseeand approximation [10]:

$$q_r = -\frac{4\sigma^*}{3m^*}\frac{\partial T^4}{\partial y}, \tag{9}$$

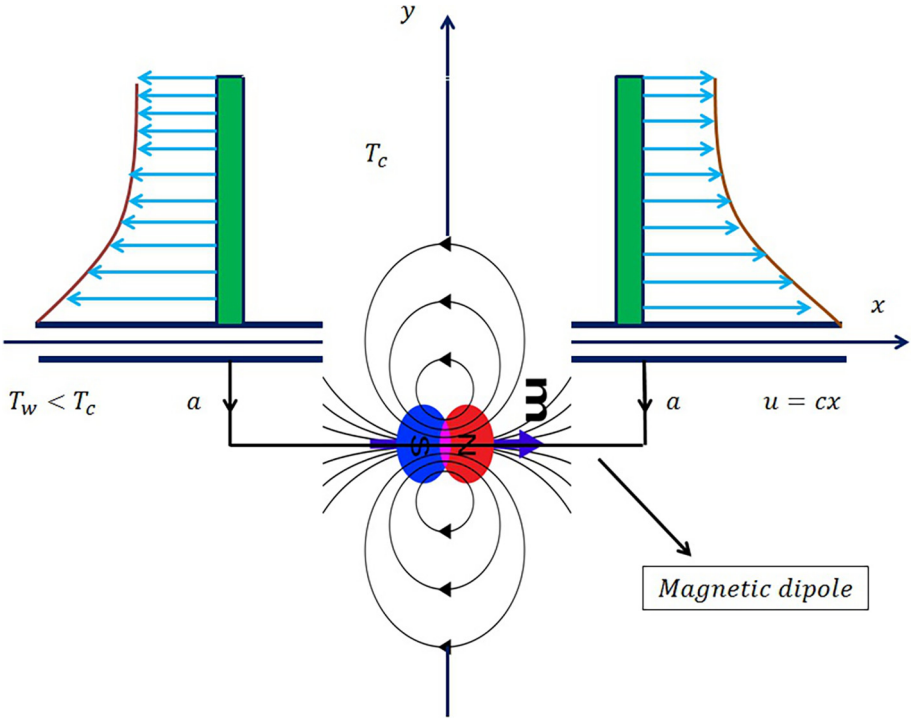

Fig. 1. Systematic diagram.

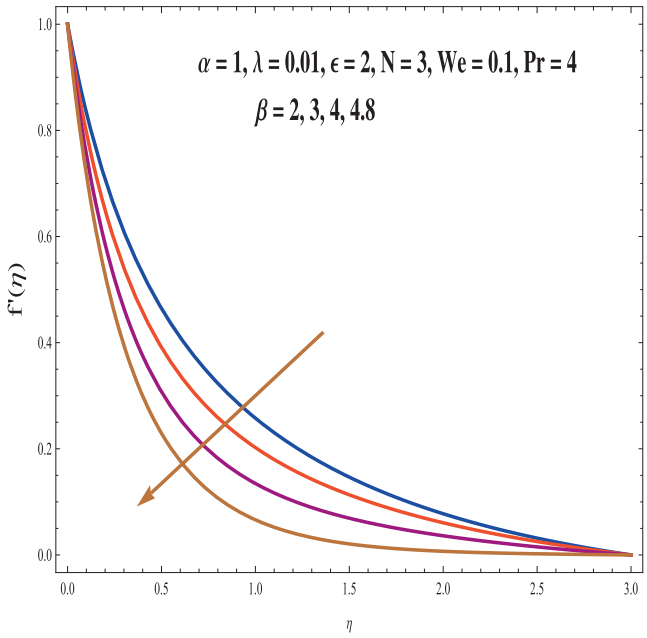

Fig. 2. $f'(\eta)$ via β.

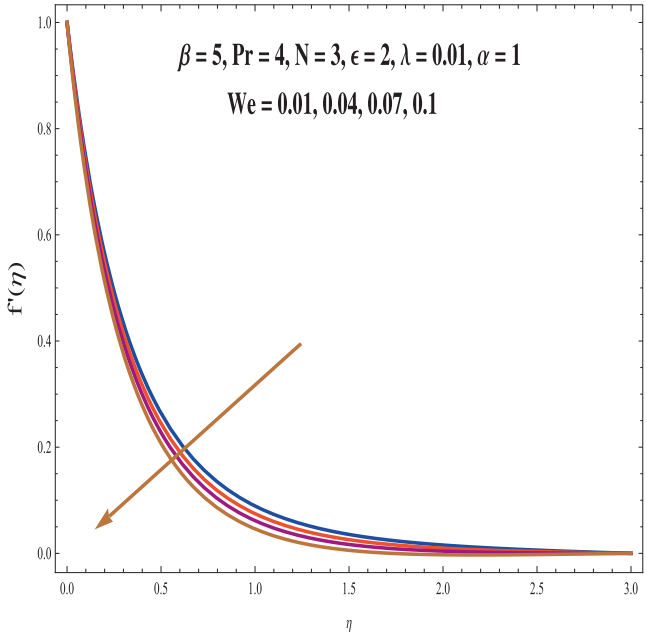

Fig. 3. $f'(\eta)$ via *We*.

we have

$$T^4 \cong 4T_c^3 T - 3T_c^4. \tag{10}$$

where δ^* represents the Stefan–Boltzmann constant and m^* the mean absorption coefficient.

Expression of magnetic scaler potential is

$$\Phi = \frac{\gamma}{2\pi}\frac{x}{x^2+(y+a)^2}. \tag{11}$$

The components of scalar potential of magnetic dipole are

$$H_x = -\frac{\partial\Phi}{\partial x} = \frac{\gamma}{2\pi}\frac{x^2-(y+a)^2}{[x^2+(y+a)^2]^2}, \tag{12}$$

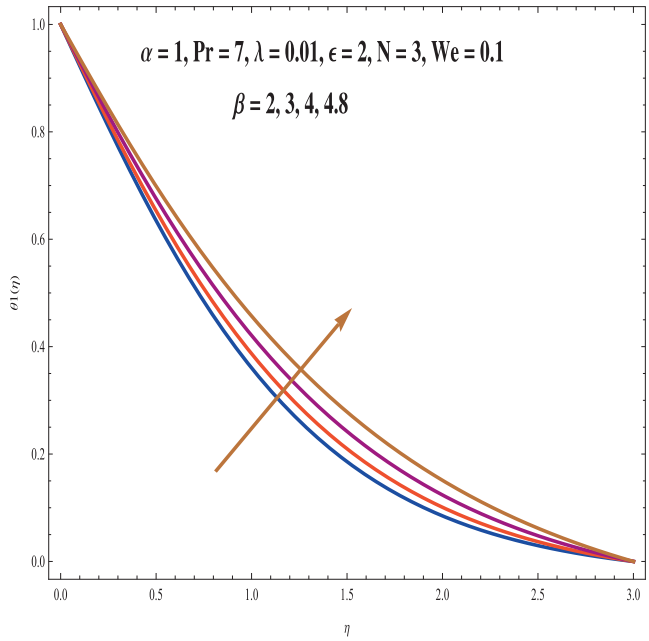

Fig. 4. $\theta_1(\eta)$ via β.

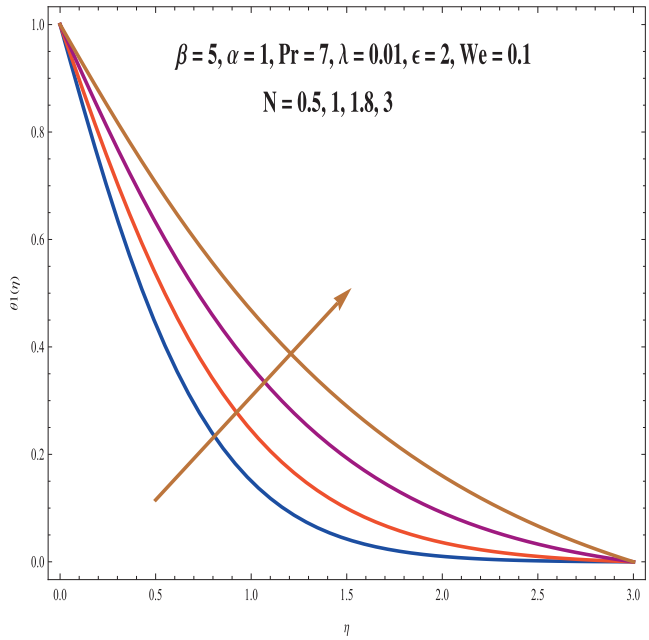

Fig. 5. $\theta_1(\eta)$ via *N*.

$$H_y = -\frac{\partial\Phi}{\partial y} = \frac{\gamma}{2\pi}\frac{2x(y+a)}{[x^2+(y+a)^2]^2}. \tag{13}$$

Magnitude of magnetic field **H** is

$$H = \left\{\left(\frac{\partial\Phi}{\partial x}\right)^2 + \left(\frac{\partial\Phi}{\partial y}\right)^2\right\}^{\frac{1}{2}}. \tag{14}$$

From Eqs. (13) and (14) we can write

$$\frac{\partial H}{\partial x} = -\frac{\gamma}{2\pi}\frac{2x}{(y+a)^4}, \tag{15}$$

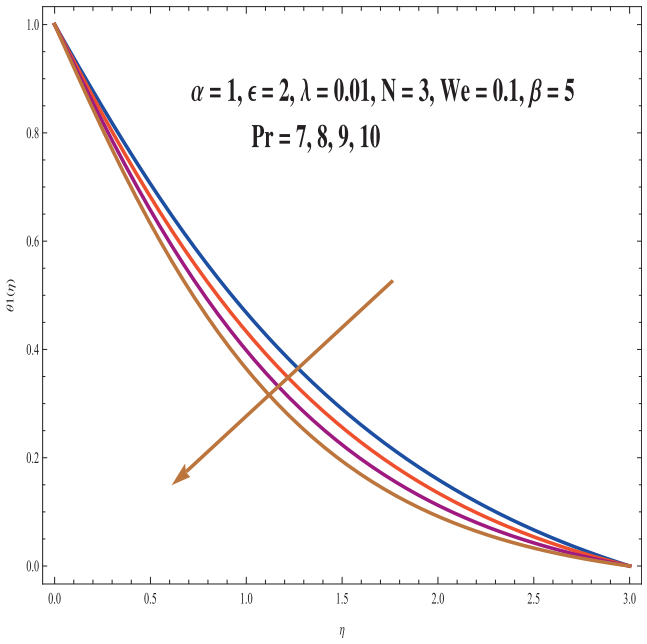

Fig. 6. $\theta_1(\eta)$ via *Pr*.

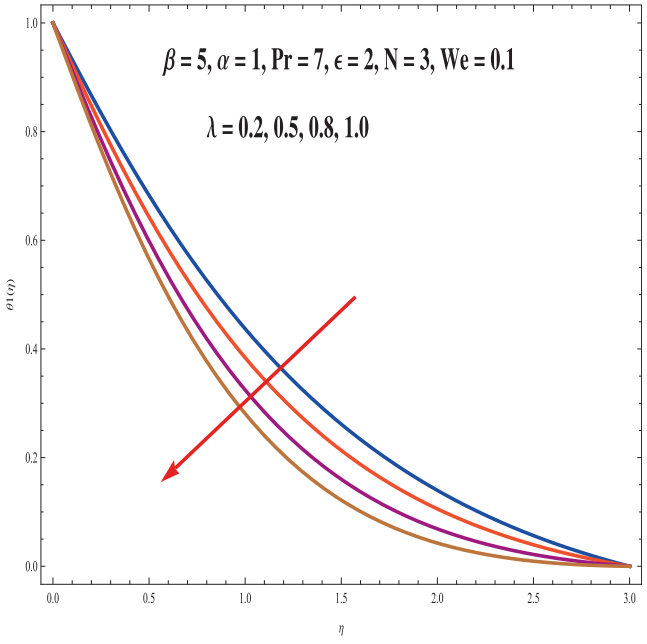

Fig. 7. $\theta_1(\eta)$ via λ.

$$\frac{\partial H}{\partial y}=\frac{\gamma}{2\pi}\left\{-\frac{2}{(y+a)^3}+\frac{4x^2}{(y+a)^5}\right\}. \tag{16}$$

The variation of magnetization (M) through temperature is

$$M=K(T_c-T), \tag{17}$$

in which K indicates pyromagnetic coefficient constant.

Transformation procedure

We consider [13]:

$$\psi(\xi,\eta)=\frac{\mu_0}{\rho}\xi f(\eta), \tag{18}$$

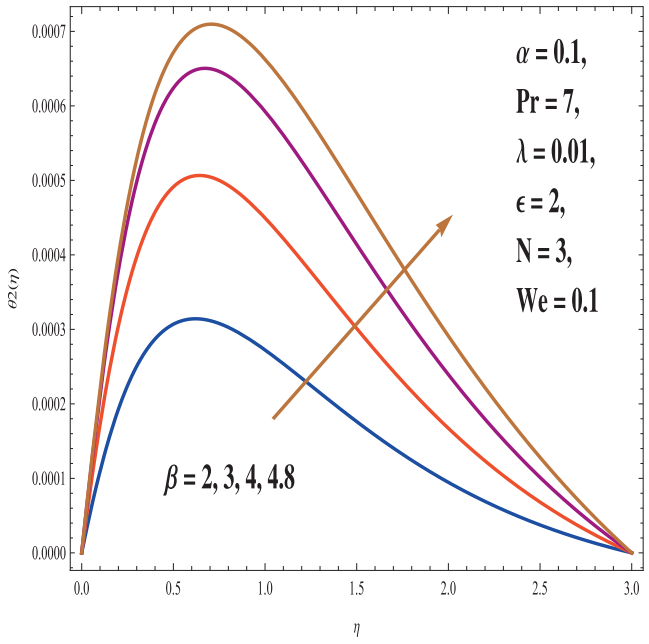

Fig. 8. $\theta_2(\eta)$ via β.

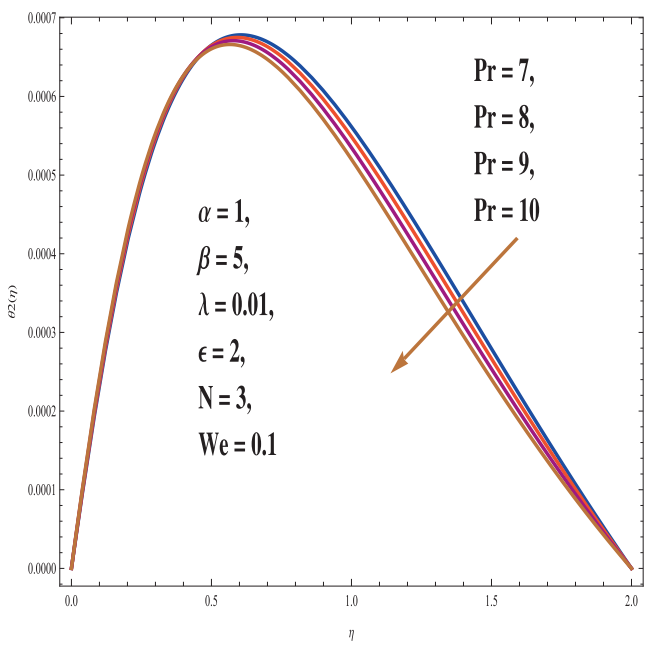

Fig. 9. $\theta_2(\eta)$ via *Pr*.

$$\theta(\xi,\eta)=\frac{T_c-T}{T_c-T_w}=\theta_1(\eta)+\xi^2\theta_2(\eta), \tag{19}$$

$$\eta=\sqrt{\frac{c\rho}{\mu_0}}y,\ \ \xi=\sqrt{\frac{c\rho}{\mu_0}}x, \tag{20}$$

with velocity components (u, v) and stream function (ψ) as

$$u=\frac{\partial\psi}{\partial y}=cxf'(\eta), \tag{21}$$

$$v=-\frac{\partial\psi}{\partial x}=-\sqrt{\frac{c\mu_0}{\rho}}f(\eta). \tag{22}$$

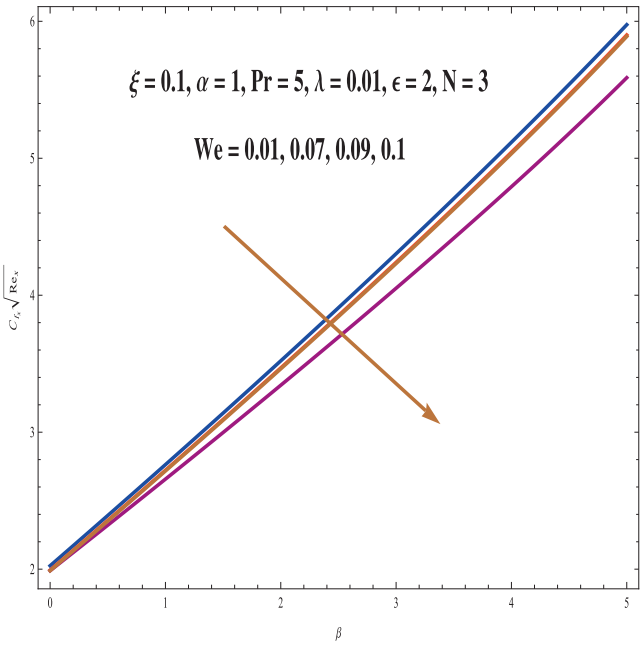

Fig. 10. Effects of β and We on C_{f_x}.

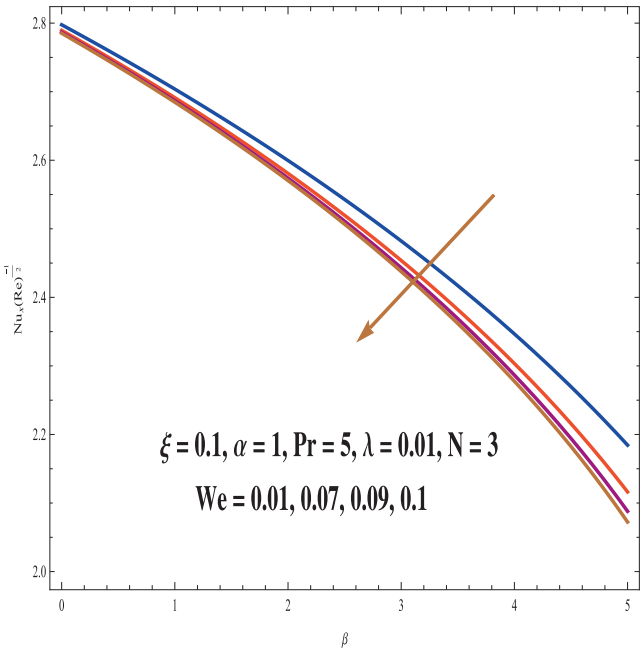

Fig. 12. Effects of β and We on Nu_x.

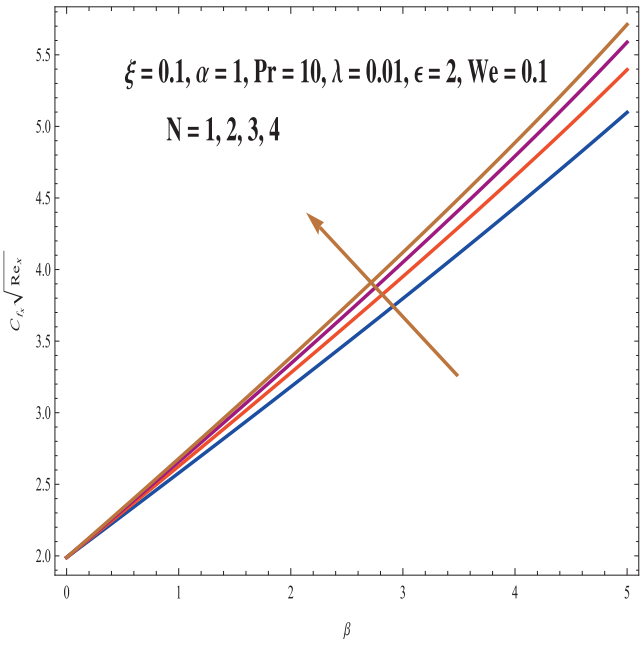

Fig. 11. Effects of β and N on C_{f_x}.

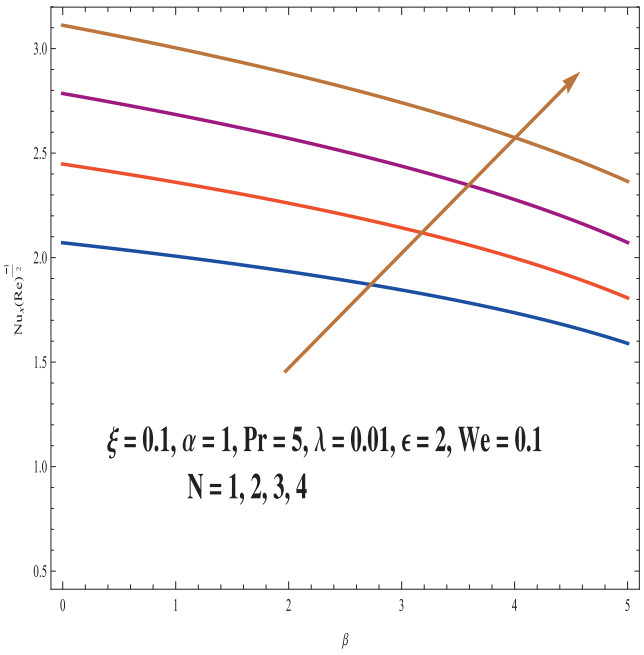

Fig. 13. Effects of β and N on Nu_x.

Note that law of conservation is automatically verified and the remaining equations takes the form

$$f''' + ff'' - (f')^2 - \frac{2\beta\theta_1}{(\eta+\alpha)^4} + Wef''f''' = 0, \tag{23}$$

$$(1+N)\theta_1'' + Prf\theta_1' + 2\lambda\beta(\theta_1 - \epsilon)\frac{f}{(\eta+\alpha)^3} = 0, \tag{24}$$

$$(1+N)\theta_2'' + Pr(\theta_2' f - 2f'\theta_2) + 2\lambda\beta\frac{\theta_2 f}{(\eta+\alpha)^3} - \lambda\beta(\theta_1 - \epsilon)\left[\frac{2f'}{(\eta+\alpha)^4} + \frac{4f}{(\eta+\alpha)^5}\right] - \lambda\left[(f'')^2 + \frac{We}{2}(f'')^3\right] = 0, \tag{25}$$

$$f(0) = 0, f'(0) = 1, \theta_1(0) = 1, \theta_2(0) = 0,$$
$$f'|_{\eta\to\infty} \to 0, \theta_1|_{\eta\to\infty} \to 0, \theta_2|_{\eta\to\infty} \to 0. \tag{26}$$

Here $Pr\left(=\frac{\mu_0 c_p}{k}\right)$ denotes the Prandtl number, $\beta\left(=\frac{\gamma\rho\lambda_0}{2\pi\mu_0^2}K(T_c - T_w)\right)$ the ferrohydrodynamic interaction, $N\left(=\frac{16\sigma^* T_c^3}{3km^*}\right)$ the thermal radiation parameter, $\epsilon\left(=\frac{T_c}{T_c - T_w}\right)$ the curie temperature, $\alpha\left(=a\sqrt{\frac{c\rho}{\mu_0}}\right)$ the dimensionless distance, $We\left(=2x\Gamma\sqrt{\frac{c^3}{\nu}}\right)$ the Weissenberg number and $\lambda\left(=\frac{c\mu_0^2}{\rho k(T_c - T_w)}\right)$ the Eckert number. Note that the combination of λ and Re_x as the

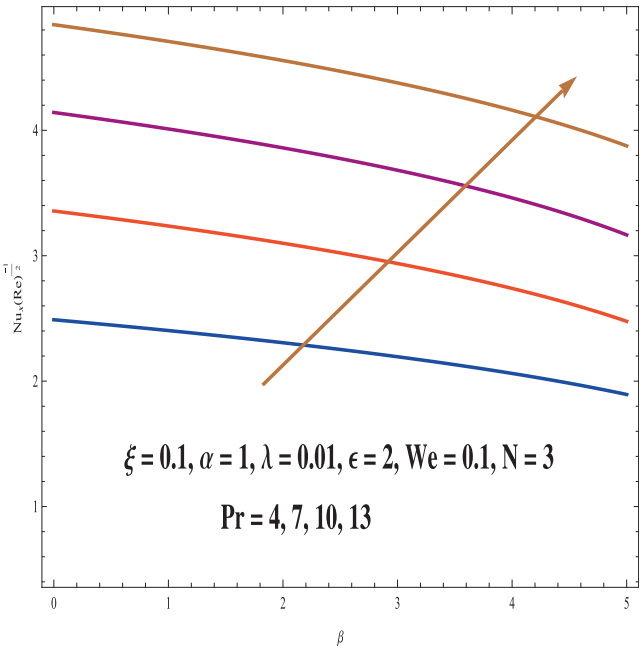

Fig. 14. Effects of β and Pr on Nu_x.

Brinkman number (combination of Eckert number and Prandtl number). This, λ is a measure of the relative importance of the viscous dissipation.

Mathematical expression for shear stress (τ_w) and heat flux q_w are

$$\tau_w = \tau_{yx}|_{y=0} = cx\mu_0\sqrt{\frac{c\rho}{\mu_0}}\left[f''(0) + \frac{We}{2}\{f''(0)\}^2\right], \tag{27}$$

$$q_w = -k\frac{\partial T}{\partial y}|_{y=0} + q_r|_{y=0}$$
$$= k(1+N)(T_c - T_w)\sqrt{\frac{c\rho}{\mu}}[\theta_1'(0) + \xi^2\theta_2'(0)]. \tag{28}$$

The dimensionless forms of (C_{f_x}) and (Nu_x) are

$$C_{f_x} = \frac{-2\tau_w}{\rho u^2} = -2\left[f''(0) + \frac{We}{2}\{f''(0)\}^2\right](Re_x)^{-\frac{1}{2}}, \tag{29}$$

$$Nu_x = \frac{xq_w}{-k(T_c - T_w)}|_{y=0} = -(1+N)[\theta_1'(0) + \xi^2\theta_2'(0)]\sqrt{Re_x}, \tag{30}$$

where $Re_x = \left(\frac{\rho cx^2}{\mu_0}\right)$ signifies the local Reynold number, C_{f_x} the skin fraction and Nu_x the heat transfer rate.

Numerical solution and discussion

The nonlinear systems (24)–(26) subject to conditions (27) are calculated numerically by Built-in-Shooting method. Further the characteristics of Prandtl number (Pr), ferromagnetic interaction (β), curie temperature (ϵ), viscous dissipation (λ), Weissenberg number (We) and thermal radiation (N) on temperature $(\theta_1(\eta), \theta_2(\eta))$, velocity $(f'(\eta))$, skin fraction $(\{f''(0) + \frac{We}{2}(f''(0))^2\}(R_{e_x})^{\frac{-1}{2}})$ and Nusselt number $(-(1+N)\{\theta_1'(0) + \xi^2\theta_2'(0)\}(R_{e_x})^{\frac{1}{2}})$ are represented in this section through Figs. 2–14. Figs. 2, 3 give the impacts of (We) and (β) on $f'(\eta)$. Here $f'(\eta)$ has decreasing behavior for larger (β). Physically with the enhancement of β the resistive force called Lorentz force increases and thus velocity field decays. Fig. 3 demonstrates the variation of Weissenberg number (We) on $f'(\eta)$. Clearly $f'(\eta)$ reduces for higher (We). It is due to the fact that relaxation time of material enhances which gives more resistance to liquid flow. Therefore velocity field and layer thickness decay. Fig. 4 is drawn to investigate the feature of (β) on temperature $\theta_1(\eta)$. Here $\theta_1(\eta)$ enhances for larger (β). Influence of radiation (N) on $\theta_1(\eta)$ is addressed through Fig. 5. A rise in temperature curves with larger thickness of boundary layer is established by increasing (N). Physically mean absorption coefficient decays for higher estimation of (N) and diffusion flux occurs because of temperature gradient which consequently increments $\theta_1(\eta)$. The curves of $\theta_1(\eta)$ for different estimations of (Pr) are presented in Fig. 6. These curves clearly indicate that temperature of liquid decreases for higher (Pr). Also thickness of boundary layer squeezed near to wall. Since, Pr and thermal diffusivity are in inverse relationship. That is why an increment in (Pr) generates lower thermal diffusivity due to which a decrease in the curves of (Pr) is noticed. Fig. 7 describes the feature of (λ) on $\theta_1(\eta)$. Here $\theta_1(\eta)$ is decreasing function of (λ). Physically thermal conductivity of liquid decays for larger (λ) and thus $\theta_1(\eta)$ decreases. Figs. 8 and 9 describe the characteristics of β and Pr on $\theta_2(\eta)$. Here $\theta_2(\eta)$ enhances for larger (β) while it decays for different estimation of (Pr). In fact the amount of resistive force enhances for (β). Therefore temperature curves enhances (see Fig. 8).

Figs. 10 and 11 demonstrate the feature of $(C_{f_x}R_{e_x}^{\frac{1}{2}})$ against $(\beta), (We)$ and (N). These graphs show that the surface drag force is enhanced with β. By increasing Weissenberg number surface drag force reduces (see Fig. 10). Fig. 11 shows that surface drag force enhances with thermal radiation (N). Influence of ferromagnetic parameter (β), Weissenberg number (We), thermal radiation (N) and Prandtl number (Pr) on heat transfer rate are described in Figs. 12–14. From these graphs it is clear that heat transfer rate reduces with (β). Fig. 12 shows that Weissenberg number reduces the heat transfer rate. Figs. 13 and 14 demonstrate that heat transfer rate enhances with thermal radiation and Prandtl number.

Conclusions

The important observations are:

- $f'(\eta)$ is reduced for larger estimations of (β) and (We).
- Temperature field enhances for larger (N) and (β) however it decays for (Pr) and (λ).
- Temperature gradient decays for (We) while it enhances by (Pr) and (N).
- Velocity gradient enhances subject to larger radiation (N) and decays for (We).

References

[1] Andersson HI, Valnes OA. Flow of a heated ferrofluid over a stretching sheet in the presence of a magnetic dipole. Acta Mech 1998;128:39–47.
[2] Titus LSR, Abraham A. Heat transfer in ferrofluid flow over a stretching sheet with radiation. Int J Eng Res Tech 2014:3. 2278:0181.
[3] Zeeshan A, Majeed A, Ellahi R. Effect of magnetic dipole on viscous ferro-fluid past a stretching surface with thermal radiation. J Mol Liq 2016;215:549–54.
[4] Sheikholeslami M, Ganji DD, Rashidi MM. J Taiwan Inst Chem Eng 2015;47:6–17.
[5] Neuringer JL. Viscous flows of a saturated ferro-fluid under the combined influence of thermal and magnetic field gradients. Int J Nonlinear Mech 1966;1:123–37.
[6] Kefayati GHR. Natural convection of ferrofluid in a linearly heated cavity utilizing LBM. J Mol Liq 2014;191:1–9.
[7] Imtiaz M, Hayat T, Alsaedi A. Convective flow of ferrofluid due to a curved stretching surface with homogeneous-heterogeneous reactions. Powder Tech 2017;310:154–62.
[8] Yasmeen T, Hayat T, Khan MI, Imtiaz M, Alsaedi A. Ferrofluid flow by a stretched surface in the presence of magnetic dipole and homogeneous-heterogeneous reactions. J Mol Liq 2016;223:1000–5.

[9] Muhammad N, Nadeem S, Haq RU. Heat transport phenomenon in the ferromagnetic fluid over a stretching sheet with thermal stratification. Res Phys 2017;7:854–61.
[10] Hayat T, Khan MI, Imtiaz M, Alseadi A, Waqas M. Similarity transformation approach for ferromagnetic mixed convection flow in the presence of chemically reactive magnetic dipole. AIP Phys Fluids 2016;28:102003.
[11] Zeeshan A, Majeed A, Ellahi R. Effect of magnetic dipole on viscous ferro-fluid past a stretching surface with thermal radiation. J Mol Liq 2016;215:549–54.
[12] Qasim M, Khan ZH, Khan WA, Shah IA. MHD boundary layer slip flow and heat transfer of ferrofluid along a stretching cylinder with prescribed heat flux. PloS One 2014;9:e83930.
[13] Hayat T, Ahmad S, Khan MI, Alseadi A. Non-Darcy Forchheimer flow of ferromagnetic second grade fluid. Res Phys 2017;7:3419–24.
[14] Shahzad A, Ali R. Approximate analytic solution for magneto-hydrodynamic flow of a non-Newtonian fluid over a vertical stretching sheet. Can J Appl Sci 2012;2:202–15.
[15] Hayat T, Khan MWA, Alsaedi A, Khan MI. Squeezing flow of second grade liquid subject to non-Fourier heat flux and heat generation/absorption. Colloid Polym Sci 2017;295:967–75.
[16] Farooq M, Khan MI, Waqas M, Hayat T, Khan MI. MHD stagnation point flow of viscoelastic nanofluid with non-linear radiation effects. J Mol Liq 2016;221:1097–103.
[17] Hayat T, Khan MI, Farooq M, Alsaedi A, Yasmeen T. Impact of Marangoni convection in the flow of carbon–water nanofluid with thermal radiation. Int J Heat Mass Transfer 2017;106:810–5.
[18] Ahmed J, Mahmood T, Iqbal Z, Shahzad A, Ali R. Axisymmetric flow and heat transfer over an unsteady stretching sheet in power law fluid. J Mol Liq 2016;221:386–93.
[19] Ahmed J, Begum A, Shahzad A, Ali R. MHD axisymmetric flow of power-law fluid over an unsteady stretching sheet with convective boundary conditions. Res Phys 2016;6:973–81.
[20] Qayyum S, Khan MI, Hayat T, Alsaedi A. A framework for nonlinear thermal radiation and homogeneous-heterogeneous reactions flow based on silver-water and copper-water nanoparticles: a numerical model for probable error. Res Phys 2017;7:1907–14.
[21] Waqas M, Khan MI, Hayat T, Alsaedi A. Numerical simulation for magneto Carreau nanofluid model with thermal radiation: a revised model. Comput Method Appl Mech Eng 2017;324:640–53.
[22] Ahmed J, Shahzad A, Begum A, Ali R, Siddiqui N. Effects of inclined Lorentz forces on boundary layer flow of Sisko fluid over a radially stretching sheet with radiative heat transfer. J Brazil Soc Mech Sci Eng 2017;39:3039–50.
[23] Hayat T, Qayyum S, Shehzad SA, Alsaedi A. Simultaneous effects of heat generation/absorption and thermal radiation in magnetohydrodynamics (MHD) flow of Maxwell nanofluid towards a stretched surface. Res Phys 2017;7:562–73.
[24] Khan MI, Alsaedi A, Shehzad SA, Hayat T. Hydromagnetic nonlinear thermally radiative nanoliquid flow with Newtonian heat and mass conditions. Res Phys 2017;7:2255–60.
[25] Williamson RV. The flow of a pseudoplastic materials. Ind Eng Chemist 1929;21:1108–11.
[26] Hayat T, Saeed Y, Asad S, Alsaedi A. Soret and Dufour effects in the flow of Williamson fluid over an unsteady stretching surface with thermal radiation. Z Naturforsch A 2015;70:235–43.
[27] Yousaf MM, Bilal S, Salahuddin T, Rehman KU. Three-dimensional Williamson fluid flow over a linear stretching surface. Math Sci Lett 2017;6:53–61.
[28] Zahra I, Yousaf MM, Nadeem S. Numerical solutions of Williamson fluid with pressure dependent viscosity. Res Phys 2015;5:20–5.
[29] Waqas M, Khan MI, Hayat T, Alsaedi A, Khan MI. Nonlinear thermal radiation in flow induced by a slendering surface accounting thermophoresis and Brownian diffusion. Eur Phys J Plus 2017;132(132):280.
[30] Hayat T, Nawaz S, Alsaedi A, Rafiq M. Influence of radial magnetic field on the peristaltic flow of Williamson fluid in a curved complaint walls channel. Res Phys 2017;7:982–90.
[31] Kumar KG, Rudraswamy NG, Gireesha BJ, Manjunatha S. Non linear thermal radiation effect on Williamson fluid with particle-liquid suspension past a stretching surface. Res Phys 2017;7:3196–202.
[32] Hayat T, Bashir G, Waqas M, Alsaedi A. MHD 2D flow of Williamson nanofluid over a nonlinear variable thicked surface with melting heat transfer. J Mol Liq 2016;223:836–44.
[33] Bhatti MM, Rashidi MM. Effects of thermo-diffusion and thermal radiation on Williamson nanofluid over a porous shrinking/stretching sheet. J Mol Liq 2016;221:567–73.
[34] Hayat T, Shafiq A, Alsaedi A. Hydromagnetic boundary layer flow of Williamson fluid in the presence of thermal radiation and Ohmic dissipation. Alex Eng J 2016;55:2229–40.
[35] Hayat T, Khan MI, Waqas M, Alsaedi A, Farooq M. Numerical simulation for melting heat transfer and radiation effects in stagnation point flow of carbon–water nanofluid. Comput Method Appl Mech Eng 2017;315:1011–24.
[36] Hayat T, Khan MI, Farooq M, Yasmeen T, Alsaedi A. Water-carbon nanofluid flow with variable heat flux by a thin needle. J Mol Liq 2016;224:786–91.
[37] Hayat T, Tamoor M, Khan MI, Alsaedi A. Numerical simulation for nonlinear radiative flow by convective cylinder. Res Phys 2016;6:1031–5.
[38] Khan MI, Hayat T, Khan MI, Alsaedi A. A modified homogeneous-heterogeneous reactions for MHD stagnation flow with viscous dissipation and Joule heating. Int J Heat Mass Transfer 2017;113:310–7.
[39] Sokolov A, Ali R, Turek S. An AFC-stabilized implicit finite element method for partial differential equations on evolving-in-time surfaces. J Comput Appl Math 2015;289:101–15.
[40] Ahmad L, Khan M, Khan WA. Numerical investigation of magneto-nanoparticles for unsteady 3D generalized Newtonian liquid flow. Eur Phys J Plus 2017;132:373. 132.